Wavelength-Dependent Hot Electron Relaxation in PVP Capped CdS/HgS/CdS Quantum Dot Quantum Well Nanocrystals

Alexander W. Schill* and Mostafa A. El-Sayed

Laser Dynamics Laboratory, Department of Chemistry and Biochemistry, Georgia Institute of Technology, 770 State Street, Atlanta, Georgia 30332

Received: May 19, 2004; In Final Form: July 7, 2004

Subpicosecond pump−probe transient absorption spectroscopy has been used to examine the probe wavelength-dependent kinetics of PVP capped CdS/HgS/CdS quantum dot quantum well nanoparticles. Using 398- and 520-nm excitations, the relaxation of the excited hot electrons above the band gap state is characterized by both rapid electronic nonradiative relaxation and slower thermal relaxation processes. The wavelength dependence of both the fast rise and fast decay of the transient bleach is discussed in terms of electronic relaxation processes involving mixed CdS/HgS states at short probe wavelengths or pure HgS states at long probe wavelengths. The slow decay of the transient bleach is discussed in terms of a thermal relaxation process leading to the dissipation of heat from the hot nanoparticle lattice to the surrounding medium.

Introduction

The interest in nanocrystalline semiconductor heterostructures was first demonstrated by the preparation of mixed ZnS/CdS and CdS/HgS colloids.[1,2] This was then followed by the preparation of the first quantum well within a quantum dot in the form CdS/HgS/CdS.[3] This new type of nanocrystalline heterostructure became known as the quantum dot quantum well (QDQW) and has since been the subject of numerous spectroscopic and photophysical studies. Experiments concerning the QDQW crystal structure,[4] luminescence properties,[5] picosecond relaxation,[6] magnetic properties,[7] and charge-carrier localization times[8] have been conducted in the past decade following its discovery.

The characteristic property of the QDQW is that it is formed of two or more semiconductor materials with large differences in band gap energy. In CdS/HgS/CdS, the core material, CdS, has a band gap energy of 2.42 eV while HgS, the well material, has a band gap energy of 0.5 eV. This band gap energy difference, combined with the layered structure of the particle, generates within the crystal a region of high local confinement within the HgS well. The behavior of excited charge carriers in such an environment has been the focus of most research being done on the QDQW system.

The sizes of CdS/HgS/CdS nanocrystals are between 5 and 6 nm in diameter. In this size regime, quantum confinement effects dominate the electronic structure and therefore the optical absorption spectrum of the particles immersed in solution. The absorption spectrum of these particles extends throughout the entire visible region from 700 to 400 nm and into the UV (Figure 1). The absorption spectrum shares many of the characteristics of the CdS spectrum, but with additional absorption due to new transitions arising from the perturbation by the HgS well monolayer. From theoretical studies of the CdS/HgS/CdS system, it is known that higher excited states are characterized by electronic wave functions that are more CdS in character, while lower excited states have more HgS character.[9−11] It is therefore possible to think about the excitation of the CdS/HgS/CdS system in terms of core excitation (producing an excited state with mostly CdS character) versus much lower energy well excitation (producing an excited state with predominately HgS character). Using fluorescence line narrowing spectroscopy, it has been demonstrated that the emission from colloidal CdS/HgS/CdS has a vibronic signature associated with the LO phonon mode of bulk HgS.[5,12] This serves as experimental confirmation of what the theory has predicted, that the lowest excited state of CdS/HgS/CdS is dominated by a HgS electronic structure. From this we can establish a model for the excited-state relaxation of the CdS/HgS/CdS system in terms of core excitation versus well excitation and in terms of hot electron relaxation from core-dominated excited states to well-dominated states near the band gap.

This model has been used previously to interpret measurements of ultrafast relaxation processes in QDQW nanocrystals.[13,8] Time-resolved pump−probe studies have revealed the behavior of transient signals resulting from electronic excitation of CdS/HgS/CdS nanocrystals. A rapid spectral diffusion from higher energy, CdS dominated bleached absorption to lower energy, HgS dominated bleached absorption occurs within the first 5 picoseconds of the relaxation. In addition to transient bleaching behavior, the rise and decay of stimulated emission from excited CdS/HgS/CdS was also investigated. Under the premise of the proposed model, the time evolution of the stimulated emission signal yields parameters associated with the migration of charge carriers into their respective lowest excited states. It is not necessarily expected that the electron and hole relax to their lowest excited states at the same rate, but the rise time of the stimulated emission signal indicates the time it takes for the slowest of the carriers to relax. To further investigate this phenomenon, Braun et al.[8] also monitored the kinetic behavior of transient signals that are only associated with hole relaxation. In particular, they used transient IR excited-state absorption spectroscopy at 4700 nm to probe the evolution of the hole relaxation independently from that of the electron. This study demonstrated that the transient signal associated with the hole shows up within 50−120 fs while the stimulated

* To whom correspondence should be addressed.

10.1021/jp047832u CCC: $27.50
Published on Web 08/18/2004

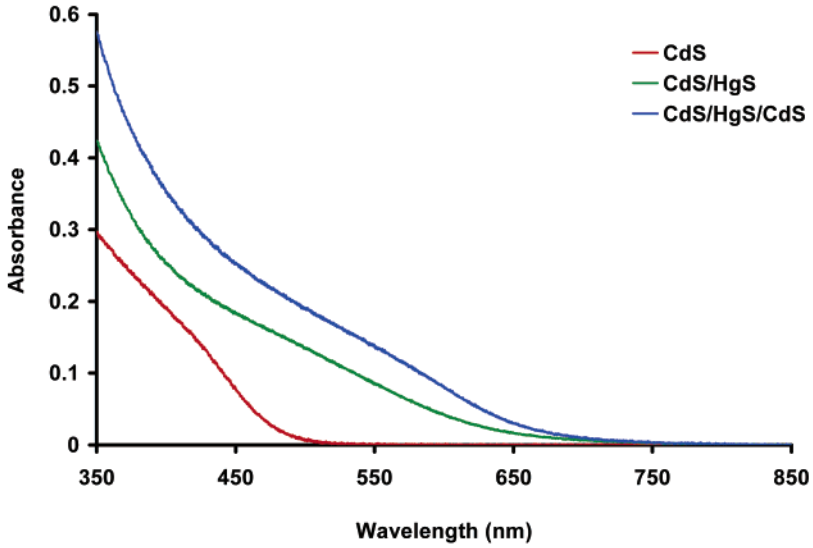

Figure 1. Absorption spectra collected during the preparation of PVP−CdS/HgS/CdS nanocrystals.

emission signal rises in 1.5 ps. It was therefore suggested that the electron is the slower of the two migrating charge carriers.[8]

The focus of the present work is to further characterize the excited hot electron relaxation of CdS/HgS/CdS nanoparticles following the introduction of PVP as a capping material. The probe wavelength-dependent relaxation kinetics are to be examined under different excitation conditions and in terms of the extent of mixing between the core CdS and well HgS states involved in the relaxation processes observed.

Experimental Section

PVP−CdS/HgS/CdS nanocrystals were prepared using a modified version of the synthesis technique that has traditionally been used.[3] The synthesis may be separated into three parts: (1) growing the CdS core, (2) exchanging the outermost Cd atoms for Hg to form the HgS well monolayer, (3) capping the well with a monolayer of CdS.

The core of CdS was synthesized in methanol using PVP (MW 50 000 Da) as a capping material. For the source of Cd^{2+}, a 0.1 M solution of $CdCl_2$ was prepared in deionized water. A 0.2 mL portion of the Cd^{2+} solution was added to 100 mL of methanol in a 250-mL three-neck reaction flask. A 0.2-mL portion of 10% PVP in methanol was also added to the reaction flask and the mixture was purged with argon gas for 30 min under vigorous stirring. Afterward, 1.0 mL of H_2S gas was rapidly injected into the sealed reaction vessel while the mixture continued to stir rapidly. After 10 min, a bright greenish-yellow solution had evolved, indicating the growth of CdS nanocrystals. This solution was then purged with argon for an additional 30 min to remove any excess H_2S gas that may have remained. A 3-mL sample of the CdS colloidal suspension was taken for analysis followed by a rapid injection of 0.1 mL of 0.1 M $HgCl_2$ in deionized water. After 5−10 s of vigorous stirring after the injection of Hg^{2+}, a 3-mL sample of the CdS/HgS colloid was removed and the remaining reaction mixture was treated with a dropwise addition of 30 mL of a 1-mL H_2S/100-mL methanol solution. The slow addition of S^{2-} is necessary to avoid the generation of high local concentrations of Cd^{2+} and S^{2-}, which could result in the formation of new CdS seeds. The slow addition process should take at least 20 min and a completed synthesis is indicated by a deep reddish-brown color of the reaction solution. After the addition of S^{2-} in the last step is complete, the reaction mixture was again purged with argon to remove any excess dissolved gas. The approximately 120 mL of CdS/HgS/CdS colloidal suspension was then transferred to a 250-mL round-bottomed flask and 1 g of PVP was added to the solution. The additional PVP ensures complete protection of the nanocrystals and also facilitates the preparation of a dry film of the QDQW sample. The 120-mL sample was concentrated to about 10 mL using a rotary evaporator and the final samples were stored in vials in the dark. Samples taken during the preparation were transferred to a 1-cm glass cuvette and characterized using UV−vis spectroscopy.

For subpicosecond pump−probe spectroscopy, the concentrated samples were filtered through a 0.1 micron syringe filter and placed into cylindrical glass cuvettes with a path length of 2 mm. Under low excitation energies (<800 nJ), the samples could be studied without rotation of the sample cell. At higher pump powers, however, the cells should be rotated to avoid local photobleaching. For all experiments, the pump pulse produced less than one electron−hole pair per particle.

Subpicosecond pump−probe transient spectroscopy was carried out using an amplified Ti:Sapphire laser system and a traditional slow-scan pump−probe optical setup. The amplified Ti:Sapphire laser (Clark-MXR CPA-1000) has an output of 0.8 mJ, 100 fs pulses at a fundamental wavelength of 795 nm. A small fraction of the beam (4%) was split and sent to a white light continuum generator while the remaining 96% was used for harmonic generation (398 and 265 nm) and the pumping of two OPAs (Quantronix TOPAS). Pump beams from either the harmonic generator or OPA were passed down a delay line and overlapped with the white light continuum beam within the sample. The spot sizes were approximately 250 micron for the pump beam and 100 micron for probe. Single wavelength kinetics were monitored using a monochromator/photodiode arrangement coupled to a boxcar integrator and a lock-in amplifier. The pump beam was chopped at 492 Hz (f/2) and used as the reference frequency for the lock-in.

Results

Absorption spectra taken during the CdS/HgS/CdS preparation are shown in Figure 1. The CdS nanocrystals show an excitonic transition at about 400 nm (3.1 eV), indicating an approximate size of 4 nm in diameter.[14] Following the addition of the HgS well layer, the spectrum red shifts to about 500 nm, and the overall extinction increases over the entire spectrum.

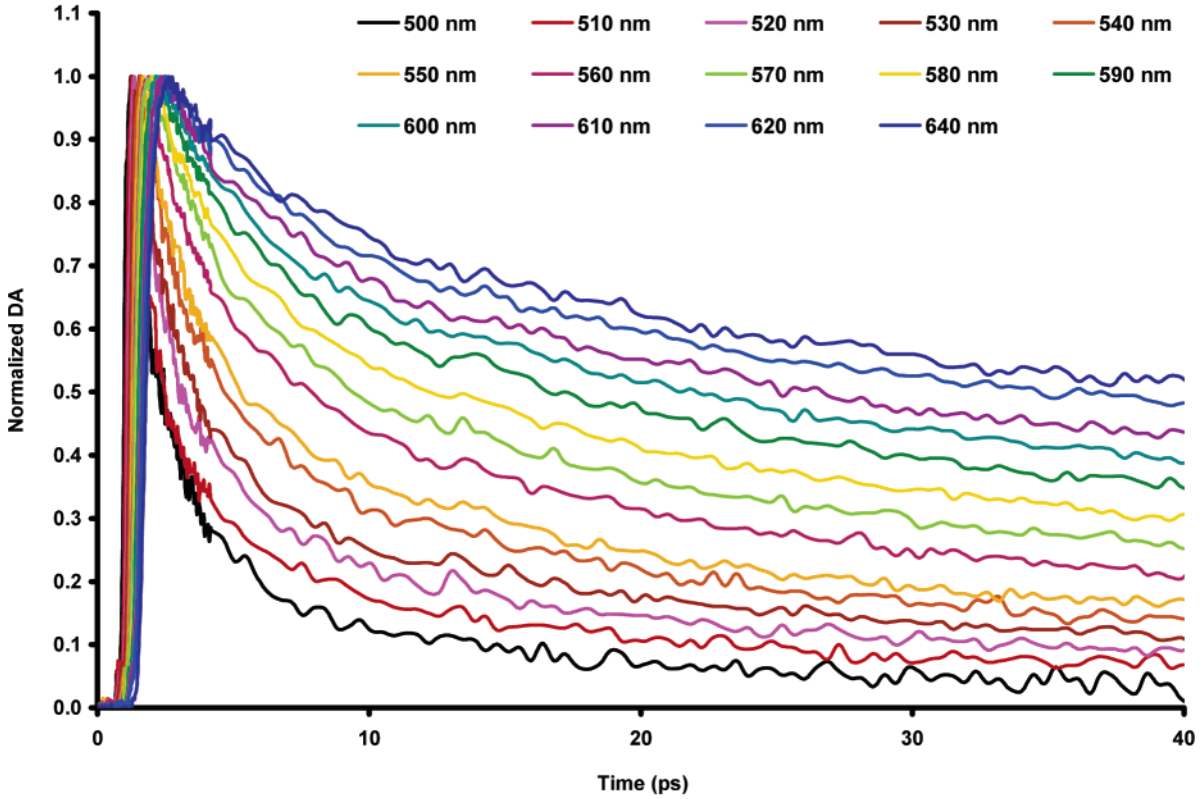

Figure 2. Pump−probe kinetic traces of excited PVP−CdS/HgS/CdS nanocrystals obtained following excitation with a 100 fs pulse of 398-nm light. Probe wavelengths indicated on the figure.

The final addition of the CdS outer layer again shifts the absorption spectrum slightly to about 560 nm, and the extinction again increases slightly. The final CdS/HgS/CdS particles are about 5 nm in diameter, assuming a layer thickness of 0.5 nm for both the HgS well and CdS outer layer and considering that the outermost layer of the CdS core was displaced by a monolayer of HgS.

Figure 2 shows the pump−probe kinetic traces of excited PVP−CdS/HgS/CdS nanocrystals obtained using 398-nm excitation and monitored at different wavelengths. The probe wavelengths selected cover the entire range of the ground-state bleach and demonstrate the differences in the bleach relaxation behavior for different transitions. As can be seen in the figure, transitions at higher energy relax much faster than lower energy transitions. A similar effect is also seen in the rise times. To obtain rise times of these kinetic traces, the experimental data shown in Figure 2 was fit using a nonlinear least-squares fitting routine. The fitting function used consisted of a multiple exponential rise and decay numerically convoluted with a 150 fs fwhm Gaussian instrument response function. To obtain acceptable fits of the rise portion of the traces, the fitting procedure was limited to the data points within the first 3 picoseconds of the signal. The best-fit curves are shown in Figure 3A. From these fit functions, the rise times were determined using the 10−90% of maximum signal methodology. The reported rise times are therefore the times taken for the signal to rise from 10% to 90% of its maximum intensity. These times are plotted as a function of probe wavelength in Figure 4A. The decay portion of the traces shown in Figure 2 were fit to a two exponential decay function and the parameters of the fit are summarized in Table 1.

Figure 3B shows the pump−probe kinetic traces recorded for excited PVP−CdS/HgS/CdS nanocrystals following excitation at 520 nm. For comparison and rise time calculations, the experimental data were again fit using a nonlinear least-squares fitting routine. The best-fit curves are plotted in Figure 3B. The rise times in Figure 3B were again determined using the 10−90% methodology and plotted as a function of probe wavelength in Figure 4B.

Discussion

Wavelength-Dependent Rise Times. Excitation of colloidal PVP−CdS/HgS/CdS at 398 nm generates hot excited electrons high above the band gap energy level. Relaxation from this initial state was monitored using pump−probe transient absorption spectroscopy at different probe wavelengths. Bleaching of ground-state absorptions in semiconductor nanocrystals can be attributed to state-filling by either the electron, the hole, or by both carriers. However, it has been shown that the observed time-dependent bleach in the visible region is attributed to the relaxation of the electron.[15] Excited states in the CdS/HgS/CdS system can be modeled as a mixing of pure CdS states with pure HgS states. The wave functions for higher excited states of CdS/HgS/CdS can be considered as having more CdS character, while the opposite is true for the lower excited states, those having more HgS character. Intermediate states are composed of a mixture of pure CdS and HgS states. The probe wavelength dependence of the pump−probe kinetics in PVP−CdS/HgS/CdS because of excited-state relaxation is expected to reflect the nature of the wave functions of these states.

Rise times of bleached absorptions from 500 to 720 nm are plotted in Figure 4. Figure 4A shows the wavelength dependence of the bleach following 398-nm excitation while Figure 4B shows the same dependence under 520-nm excitation conditions. In Figure 4A, there is a steady increase in the rise times between 500 and 620 nm, followed by a constant between 620 and 720

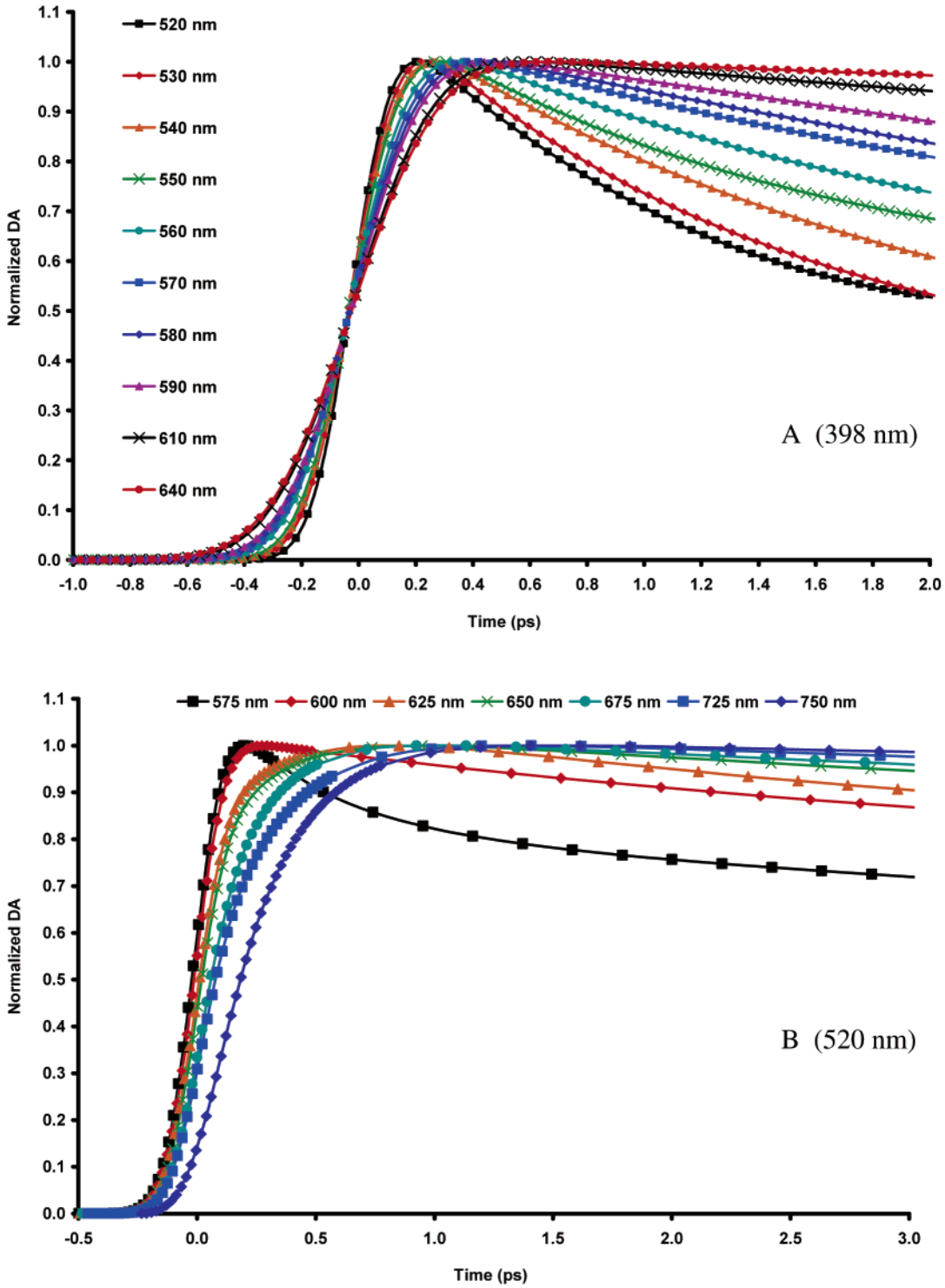

Figure 3. Pump−probe kinetic traces of excited PVP−CdS/HgS/CdS nanocrystals obtained following excitation with 100 fs pulses of 398 (A) and 520 (B) nm light. The traces shown are chirp-adjusted best-fit curves to the experimental data.

nm. Since bleached absorptions in this region are associated with electron relaxation, the rise time of the bleach is proportional to the relaxation time of the electron from the higher excited state at 398 nm (3.1 eV) to a particular state monitored at a longer wavelength (lower energy). The higher energy absorptions involve states whose wave functions are more similar to that of the initially prepared state and have mostly CdS character. The states monitored using probe wavelengths between 500 and 620 nm are mixtures of CdS and HgS states. The states monitored at wavelengths longer than 620 nm are those of the HgS well. This qualitative picture is represented graphically in Scheme 1.

Following excitation at 520 nm, the rise times of the bleach increase steadily across the entire spectrum of bleached absorptions (Figure 4B). In contrast to the wavelength dependence for 398-nm excitation, there is not any sign of leveling off to a constant rise time for the bleach resulting from 520-nm excitation.

A qualitative explanation of this is that the prepared state at 520 nm is a CdS/HgS mixed state. Its relaxation to other mixed

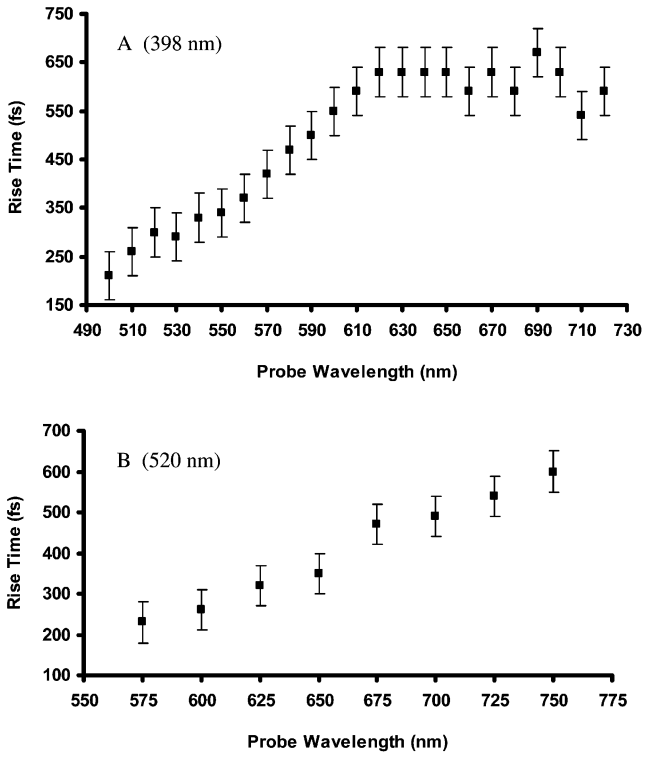

Figure 4. Rise times of the transient signal at various probe wavelengths for PVP−CdS/HgS/CdS nanocrystals following excitation with 100 fs pulses of 398 (A) and 520 (B) nm light. Rise times were determined from the best-fit curves to the experimental data using the 10−90% method. The uncertainty in these times is ±50 fs and indicated by the error bars.

states or pure HgS states must always be described using cross terms involving states in the two materials.

The above qualitative explanation can be formulated quantum mechanically as follows. Assume that the wave functions of any excited state in CdS/HgS/CdS nanoparticles can be written as

$$\psi_\lambda = \alpha_\lambda^{\mathrm{CdS}}\psi^{\mathrm{CdS}} + (1-\alpha_\lambda^{\mathrm{CdS}})\psi^{\mathrm{HgS}} \quad (1)$$

where ψ^{CdS} and ψ^{HgS} are the wave functions for pure CdS and pure HgS, respectively. The wavelength-dependent coefficient α_λ determines the fraction of CdS character within the mixed CdS/HgS wave function for a state monitored at wavelength λ. Pure CdS states would therefore have α_λ equal to 1 while pure HgS would have α_λ equal to 0. Mixed states would then of course have α_λ between 0 and 1. Given this expression for the wave functions of the CdS/HgS/CdS system, another expression can be written for the relaxation rate between an initial state, $\psi_{\lambda\mathrm{pump}}$ and a final state $\psi_{\lambda\mathrm{probe}}$ using Fermi's golden rule,

$$\omega_{\psi_{\lambda\mathrm{pump}},\psi_{\lambda\mathrm{probe}}} = \frac{1}{\tau^{\mathrm{rise}}_{\lambda\mathrm{probe}}} = |\langle\psi_{\lambda\mathrm{pump}}H\psi_{\lambda\mathrm{probe}}\rangle|^2\frac{\rho_{\lambda\mathrm{probe}}}{\hbar} \quad (2)$$

where the initial state is labeled with the subscript λ_{pump} and the final state carries the subscript λ_{probe}, H is the perturbing Hamiltonian responsible for coupling and relaxation between the two states, and ρ is the density of the final state. This expression describes the dynamics of relaxation from the initial state generated by optical excitation at λ_{pump} to the state monitored by the probe wavelength λ_{probe}. This will be used to interpret the results obtained for the wavelength-dependent transient bleach rise times with λ_{pump}= 398 nm and λ_{pump}= 520 nm.

TABLE 1: Wavelength-Dependent Kinetic Decay Parameters Determined from Fitting the Experimental Data Traces Obtained Using 398-nm Excitation[a]

probe wavelength (nm)	*T*1 (ps)	% *T*1	*T*2 (ps)	% *T*2
500	0.8	64	7	36
510	1.0	65	16	35
520	1.5	80	24	20
530	1.8	69	34	31
540	2.2	62	36	38
550	2.5	58	40	42
560	3.2	55	47	45
570	3.6	50	56	50
580	4.2	47	64	53
590	4.4	41	69	59
600	4.7	39	77	61
610	5.1	36	85	64
620	6.0	29	95	71
630	5.9	33	107	67
640	6.0	30	115	70
650	6.0	27	115	73
660	6.0	22	119	78
670	6.0	28	121	72
680	6.0	26	128	74
690	6.0	26	134	74
700	6.0	28	140	72
710	6.0	23	158	77
720	6.0	33	160	67

[a] The data were fit to a two exponential decay function. Time constants for the fast (*T*1) and slow (*T*2) decay components are shown along with the percent relative amplitudes of each.

SCHEME 1: Graphical Representation of the Relaxation Model Used for the Interpretation of Experimental Data[a]

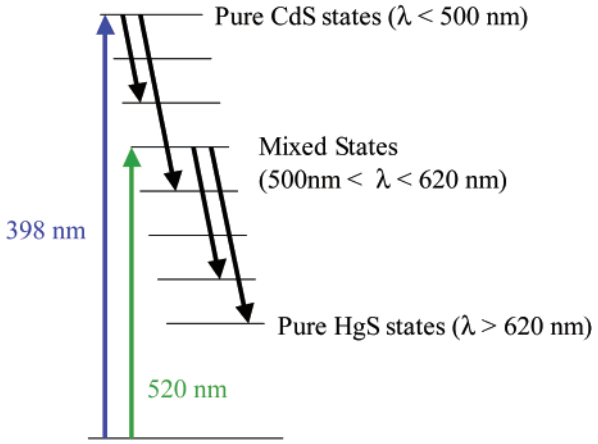

[a] Blue and green arrows represent excitation at 398 and 520 nm, respectively. Black arrows indicate the intraband relaxation from higher excited states of which the relaxation rate is proportional to the rise times given in Figure 4A and B.

With 398-nm excitation, the initial state is made up almost entirely of pure CdS wave functions while the initial state prepared by 520-nm excitation is likely a mixed state consisting of contributions of pure CdS and pure HgS wave functions. The relaxation from the initial state at 398 nm to a bleach monitored at 500 nm involves relaxation from a state that is entirely CdS in character to one that is mixed CdS/HgS in character. Equation 2 can be rewritten as

$$\omega_{398\rightarrow500\mathrm{nm}} = \frac{1}{\tau^{\mathrm{rise}}_{500\mathrm{nm}}} = |\langle\psi_{398\mathrm{nm}}H\psi_{500\mathrm{nm}}\rangle|^2\frac{\rho_{500\mathrm{nm}}}{\hbar} \quad (3)$$

for the relaxation rate from the initial state at 398 nm to the

first bleached absorption at 500 nm. However, from eq 1 it can be supposed that the wave function ψ_{500nm} is mixed in character, having a value of α_λ between 0 and 1. As the probe wavelength increases, the fraction of HgS in the mixed state increases, α_λ becomes closer to zero, the matrix element in eq 2 becomes smaller, and the result is an increase in rise time across the wavelength range 500−620 nm. Above 620 nm, the states composing the bleached absorptions are entirely HgS in character, α_λ equals zero, and the relaxation times from the initial state and corresponding rise times remain constant. Returning to the expression for the relaxation rate,

$$\omega_{398\rightarrow>620nm} = \frac{1}{\tau^{rise}_{>620nm}} = |\langle\psi_{398nm} H \psi_{>620nm}\rangle|^2 \frac{\rho_{>620nm}}{\rho} \quad (4)$$

this time writing for a bleached absorption at a wavelength greater than 620 nm. Since the bleach above 620 nm involves states that are entirely HgS in character, in other words $\psi_{>620nm}$ equals ψ^{HgS}, and the initial state at 398 nm is pure CdS in character, the above expression can be written more simply as

$$\omega_{398\rightarrow>620nm} = |\langle\psi^{CdS} H \psi^{HgS}\rangle|^2 \frac{\rho_{HgS}}{\hbar} = \omega_{\psi CdS,\psi HgS} \quad (5)$$

The constant rise time across the region 620−720 nm (∼610 fs) therefore reflects the intrinsic relaxation time from a pure CdS state to a pure HgS state in PVP−CdS/HgS/CdS nanocrystals, that is, the electronic interfacial crossing time between the two materials. The crossing time of 0.61 ps determined in the present work may be compared with the value of 1.5 ps determined from the rise time of the stimulated emission when excited at 400 nm in mercaptoacetic acid capped CdS/HgS/CdS quantum dot quantum wells of 6 nm in size.[8] The difference between these two values arises most likely from differences in the size of particles and the experimental methods used rather than a significant effect of capping material or solvent.

The relaxation from the initial state prepared with 520-nm excitation involves relaxation from a mixed CdS/HgS state to another mixed state (bleach at 575−620 nm) and eventually to a purely HgS state (bleach above 620 nm). In this case, the initial state is a mixed state of constant coefficients while the final state is either a mixed state of probe wavelength-dependent coefficients or a pure HgS state. From the gradual increase in the rise times from 200 to 600 fs, it can be suggested that one of the factors involved in the relaxation from the 520-nm initial state is the decrease in the CdS character of the states composing the bleached absorptions from 575 to 750 nm. Even though the 520-nm initial state is a mixed state, it probably has a larger fraction of CdS than HgS and will relax more rapidly into mixed states that also have larger fractions of CdS character. As the probe wavelength increases from 575 to 750 nm, the fraction of CdS character steadily drops off to zero. Under this argument, it might be expected that a leveling off of the rise time should still be observed. However, given that within the bandwidth of the laser pulses used (∼4 nm), a coherent ensemble of initial mixed states with slightly different CdS and HgS compositions is produced that will each relax in slightly different ways. In addition, inhomogeneous broadening also affects the mixed states monitored for particles of different sizes. Thus, when the excited initial state itself is a mixed state, the resolution of the monitored state becomes more difficult.

Wavelength-Dependent Decay Times. For wavelength-dependent decay measurements, excitation was carried out at 398 nm. The probe wavelength-dependent decay times are shown in Figure 5. The decay traces for the bleached transitions at different probe wavelengths were fit to a two exponential decay function and the two components are plotted separately in Figure 5A and 5B. The fast component follows the same functional dependence as the rise times, increasing over the range 500−620 nm and then leveling off over the range 620−720 nm. On the other hand, the second, slow decay component increases consistently over the whole spectrum of the bleached absorptions. This suggests that the two decay times are attributed to different relaxation pathways within the CdS/HgS/CdS system.

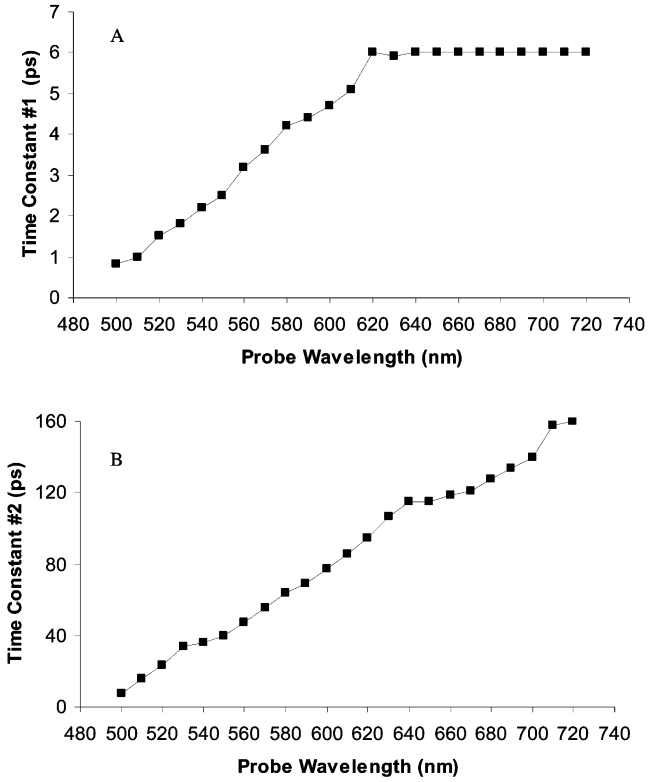

Figure 5. Probe wavelength-dependent decay times for the fast (A) and slow (B) components of the bleach recovery following excitation at 398 nm. The results were obtained by fitting the experimental kinetics traces to a two exponential decay using a nonlinear least-squares fitting routine. The fast component has been assigned to rapid electronic nonradiative relaxation while the slow component has been assigned to a thermal relaxation process.

Since the probe wavelength-dependent function for the fast time constant is very similar to that of the rise times, a similar argument for the relaxation mechanism can be made for this decay as was made for the rise. As a result of the analysis of the rise times, it was established that the mechanism behind the relaxation of excited CdS/HgS/CdS could be evaluated in terms of the relationship between the initial and final states. The wavelength-dependent rise time function identified regions of the bleach spectrum that are associated with states that were either mixed CdS/HgS or pure HgS in character.

Using the mixed wave function formalism of eq 1, the fast component decay rate of a particular bleached absorption at a monitoring wavelength λ can be expressed as

$$\left(\frac{1}{\tau}\right)_\lambda = \alpha_\lambda^{CdS} \frac{1}{\tau_{CdS}} + (1 - \alpha_\lambda^{CdS}) \frac{1}{\tau_{HgS}} \quad (6)$$

assuming that the decay rate will be a wavelength-dependent function of the decay rates of pure CdS states and pure HgS states. For bleached absorptions above 620 nm, the decaying

state is pure HgS and α_λ equals 0. For bleached absorptions below 620 nm, the decaying state is a mixture whose composition (determined by the α_λ value) is wavelength-dependent. The observed wavelength dependence of the fast decay component suggests that the excited electron decays faster in states with more CdS character. In other words, $\tau_{CdS} < \tau_{HgS}$ in eq 6. The idea that excited electrons relax faster in CdS than in HgS is understandable considering that there is many more Cd atoms than Hg atoms in these CdS/HgS/CdS nanoparticles. The number of phonons, defects, surface states, and the density of the hole states are all much larger in the CdS system than in the protected HgS well. Therefore, any of the proposed electronic nonradiative relaxation mechanisms, whether by electron−phonon coupling, by defects or surface states,[16] or by electron−hole coupling,[17] would predict that electrons in CdS would relax faster than electrons in the HgS well.

The long decay component must be explained in a different way. In this case, the probe wavelength dependence does not level off to a constant value but instead increases steadily over the entire spectrum of bleached absorptions. Also, these decay times are much larger than those of the first time constants, indicating a different type of nonradiative relaxation mechanism. Electronic nonradiative relaxation occurs on a faster time scale, so it is most probable that the relaxation process involved for the slow component is not electronic but rather involves cooling of the hot lattice by heating the surrounding medium. Hot electrons generated by the excitation pulse dissipate energy as heat to the phonons of the lattice. The hot particle lattice must then dissipate heat to the surrounding bath: capping material and solvent. Since electronic relaxation is not involved, the electronic composition of the relaxing state is immaterial and the only parameter affecting the relaxation rate is the amount of heat to be dissipated and the coupling mechanism involved between the particle surface and the heat bath (surrounding medium). The rate-limiting step for relaxation by this mechanism is the cooling of the particle lattice by heat transfer to the surrounding bath. The rate of heat loss is directly proportional to the temperature difference between the two media and will occur faster for a hotter lattice resulting from the relaxation of a higher energy excited electron. Hot electrons in bleached states that are closer to the initial state are expected to produce more vibrational energy when they relax than lower energy states and are therefore responsible for more heating of the lattice. Thus, assuming that the coupling between the nanoparticle and the surrounding medium is the same and that the type of relaxation is not rate-determined by the heat conductivity of the medium, the observed functional dependence of the relaxation time on monitoring wavelength (excited electron energy) can be understood.

References and Notes

(1) Haesselbarth, A.; Eychmueller, A.; Eichberger, R.; Giersig, M.; Mews, A.; Weller, H. *J. Phys. Chem.* **1993**, *97*, 5333−5340.

(2) Henglein, A. *Top. Curr. Chem.* **1988**, *143*, *115*, 131.

(3) Eychmueller, A.; Mews, A.; Weller, H. *Chem. Phys. Lett.* **1993**, *208*, 1, 59−61.

(4) Mews, A.; Eychmueller, A.; Giersig, M.; Schooss, D.; Weller, H. *J. Phys. Chem.* **1994**, *98*, 934−941.

(5) Mews, A.; Kadavanich, A. V.; Banin, U.; Alivisatos, A. P. *Phys. Rev. B* **1996**, *53*, *20*, 13242−13244.

(6) Kamalov, V. F.; Little, R. B.; Logunov, S.; El-Sayed, M. A. *J. Phys. Chem.* **1996**, *100*, *16*, 6381−6384.

(7) Lifshitz, E.; Porteanu, H.; Glozman, A.; Weller, H.; Pflughoeft, M.; Eychmueller, A. *J. Phys. Chem. B* **1999**, *103*, 6870−6875.

(8) Braun, M.; Link, S.; Burda, C.; El-Sayed, M. A. *Phys. Rev. B* **2002**, *66*, *20*, 205312−205317.

(9) Schooss, D.; Eychmueller, A.; Mews, A.; Weller, H. *Phys. Rev. B* **1994**, *49*, *24*, 17072−17078.

(10) Bryant, G. W.; Jaskolski, W. *Phys. Status Solidi* **2001**, *224*, *3*, 751−755.

(11) Perez-Conde, J.; Bhattacharjee, A. K. *Phys. Status Solidi* **2002**, *229*, *1*, 485−488.

(12) Eychmueller, A.; Mews, A. *Ber. Bunsen-Ges. Phys. Chem.* **1998**, *102*, 1343−1357.

(13) Braun, M.; Burda, C.; Mohamed, M.; El-Sayed, M. A. *Phys. Rev. B* **2001**, *64*, *3*, 35317.

(14) Vossmeyer, T.; Katsikas, L.; Giersig, M.; Popovic, I. G.; Diesner, K.; Chemseddine, A.; Eychmueller, A.; Weller, H. *J. Phys. Chem.* **1994**, *98*, 7665−7673.

(15) Klimov, V. I. *J. Phys. Chem. B* **2000**, *104*, 6112−6123.

(16) Darugar, Q.; Landes, C.; Link, S.; Schill, A.; El-Sayed, M. A. *Chem. Phys. Lett.* **2003**, *373*, *3*, *4*, 284−291.

(17) Efros, Al L.; Kharchenko, V. A.; Rosen, M. *Solid State Commun.* **1995**, *93*, *4*, 281−4.